of Λ(calcd) in Table III were obtained by using eq 1 with x = 0.008 45 and Λ_{25} = 3.46 cm^2 mol^{-1} Ω^{-1}. The difference between Λ and Λ(calcd) in Table III is due to the existence of the second species.

Discussion

The temperature dependence of the ^{1}H NMR line width shows that, as in the case of $TiCl_3$–CH_3CN, two species exist in solutions of VCl_3 in CH_3CN. The temperature dependence of the equivalent conductivity lends support to this idea. The low values of the equivalent conductivity at all temperatures show that not much ionization occurs. Thus, the two species present must be *fac*- and *mer*-VCl_3·$3CH_3CN$. It has been established by ESR measurements that at low temperatures the *fac* isomer is present in the $TiCl_3$–CH_3CN system.[7,10] It is likely that the same holds for VCl_3 in CH_3CN. It the amount of the *mer* isomer increases, the conductivity should increase slightly since this isomer and its ions are expected to be more mobile than the more polar *fac* species.[11] This is in agreement with the shape of the curve shown in Figure 2.

(10) Giggenbach, W.; Brubaker, C. H., Jr. *Inorg. Chem.* **1969**, *8*, 1131.
(11) Carassiti, V. *Gazz. Chim. Ital.* **1954**, *84*, 405.

Contribution from the Department of Chemistry,
Northeastern University, Boston, Massachusetts 02115

Stoichiometry and Kinetics of the Low-Temperature Oxidation of $L_2Cu_2Cl_2$ (L = *N,N,N′,N′*-Tetraethylethylenediamine) by Dioxygen in Methylene Chloride and Properties of the Peroxocopper Products

Geoffrey Davies,* Mohamed A. El-Sayed,*† and Maher Henary

Received October 21, 1986

The dimeric copper(I) complex LCu(Cl,Cl)CuL (D; L is *N,N,N′,N′*-tetraethylethylenediamine) completely reduces dioxygen at ambient temperatures in aprotic solvents to give the green, dimeric oxocopper(II) complex LCu(Cl,O,Cl)CuL (C). This study shows that C is the primary oxidation product at temperatures above −26 °C but that two forms of a blue, tetranuclear, mixed-valence peroxocopper complex, A and B, exist in equilibrium at lower temperatures. The blue products were characterized by electronic, ESR, and Raman spectroscopy and by kinetic measurements. Observations that the rate of conversion of A and B to C is critically dependent on temperature in the range ca. −40 to ca. −30 °C are explained by assigning $\Delta H_{11}^{\ddagger}$ = 25 ± 0.5 kcal mol^{-1} and $\Delta S_{11}^{\ddagger}$ = 40 ± 3 cal deg^{-1} mol^{-1} to this process. Copper complexes A, B, and C initiate the oxidative coupling of 2,6-dimethylphenol by dioxygen. Studies of the catalytic oxidation of excess phenol at −45, −25, and 0 °C show that the proportion of the diphenoquinone product increases very sharply at −45 °C, strongly suggesting that a catalytic cycle involving D/A,B species is responsible for this change of product distribution.

Introduction

Catalysis of dioxygen reactions by the copper(I)–copper(II) couple requires at least partial dioxygen reduction by copper(I).[1-7] Recent reviews[5,6] demonstrate substantial progress in understanding aprotic copper(I)–dioxygen chemistry in the absence of substrates. The primary stoichiometries with oxidation-resistant[6,7] ligands on copper are eq 1–5 (ligands omitted), where Cu^I, Cu^I_2

$$2[Cu^I]^+ + O_2 \rightleftarrows [Cu^{II}O_2Cu^{II}]^{2+} \quad (1)$$

$$[Cu^I_2]^{2+} + O_2 \rightleftarrows [Cu^{II}O_2Cu^{II}]^{2+} \quad (2)$$

$$4Cu^I + O_2 \rightarrow Cu^{II}_4O_2 \quad (3)$$

$$2Cu^I_2 + O_2 \rightarrow Cu^{II}_4O_2 \quad (4)$$

$$2Cu^I_2 + O_2 \rightarrow 2Cu^{II}_2O \quad (5)$$

and Cu^I_4 represent copper(I) monomers, dimers, and tetramers, respectively.

Equation 1 was observed by Wilson et al. at ambient temperatures.[8] Particular ligand systems create cationic dioxygen carriers with respectable repeat cycling reproducibility.[8] Karlin et al.[5,9-11] have designed copper(I) dimers containing two N_3Cu^+ centers that also reversibly bind dioxygen, eq 2, but only at low temperatures. Thompson[12] has even isolated blue, solid $[(TEED)Cu(O_2,H_2O)Cu(TEED)](ClO_4)_2$ (TEED is *N,N,N′,N′*-tetraethylethylenediamine), which has an absorption maximum at 630 nm and shows clear evidence for bound peroxide in its ir spectrum.

The copper systems in all of this work[4,8-12] have copper–copper distances that are large enough to accommodate μ(1,2)-peroxo bridges, as also appears to be the case in oxyhemocyanins and oxytyrosinases.[4,5]

The positive charges on the species in eq 1 and 2 probably inhibit reduction by $[Cu^I]^+$ and $[Cu^I_2]^{2+}$, respectively (eq 6). Steric bulk

$$[Cu^{II}O_2Cu^{II}]^{2+} + [Cu^I_2]^{2+} \rightarrow 2[Cu^{II}_2O]^{2+} \quad (6)$$

† On leave of absence from the Department of Chemistry, Faculty of Science, Alexandria University, Alexandria, Egypt.

(1) For an excellent collection of papers on many important aspects of copper chemistry see: *Biological and Inorganic Copper Chemistry*; Karlin, K. D., Zubieta, J., Eds.; Adenine: Guilderland, NY, **1986**; Vol. 1 and 2.
(2) Davies, G.; El-Sayed, M. A. In *Copper Coordination Chemistry: Biochemical and Inorganic Perspectives*; Karlin, K. D., Zubieta, J. A., Eds.; Adenine: Guilderland, NY, **1983**, p 281.
(3) Speier, G.; Tyeklár, Z. In *Biological and Inorganic Copper Chemistry*; Karlin, K. D.; Zubieta, J., Eds.; Adenine: Guilderland, NY, 1986; Vol. 2, p 91.
(4) Wilcox, D. E.; Porras, A. G.; Hwang, Y. T.; Lerch, K.; Winkler, M. E.; Solomon, E. I. *J. Am. Chem. Soc.* **1985**, *107*, 4015 and references therein.
(5) Karlin, K. D.; Gultneh, Y. *J. Chem. Educ.* **1985**, *62*, 983 and references therein; Karlin, K. D.; Gultneh, Y. *Prog. Inorg. Chem.*, in press.
(6) Davies, G.; El-Sayed, M. A. *Comments Inorg. Chem.* **1985**, *4*, 151.
(7) Davies, G.; El-Shazly, M. F.; Kozlowski, D. R.; Kramer, C. E.; Rupich, M. W.; Slaven, R. W. *Adv. Chem. Ser.* **1979**, *No. 173*, 178.
(8) Goodwin, J. A.; Stanbury, D. M.; Wilson, L. J. in *Biological and Inorganic Copper Chemistry*; Karlin, K. D.; Zubieta, J., Eds.; Adenine: Guilderland, NY, 1986; Vol. 2, p 11 and references therein.
(9) Karlin, K. D.; Cruse, R. W.; Gultneh, Y.; Hayes, J. C.; Zubieta, J. *J. Am. Chem. Soc.* **1984**, *106*, 3372.
(10) Karlin, K. D.; Cruse, R. W.; Gultneh, Y.; Hayes, J. C.; McKown, J. W.; Zubieta, J. In *Biological and Inorganic Copper Chemistry*; Karlin, K. D.; Zubieta, J., Eds.; Adenine: Guilderland, NY, 1986; Vol. 2, p 101.
(11) Karlin, K. D.; Haka, M. S.; Cruse, R. W.; Gultneh, Y. *J. Am. Chem. Soc.* **1985**, *107*, 5828.
(12) Thompson, J. S. In *Biological and Inorganic Copper Chemistry*; Karlin, K. D.; Zubieta, J., Eds.; Adenine: Guilderland, NY, 1986; Vol. 2, p 1 and references therein.

0020-1669/87/1326-3266$01.50/0

of the respective ligands and low concentrations of free $[Cu^I]^+$ and $[Cu^I_2]^{2+}$ (because of large equilibrium constants in eq 1 and 2)[8-11] are other probable stabilizing factors. Disproportionation reaction 7 would be slower at lower peroxocopper(II) concen-

$$2[Cu^{II}O_2Cu^{II}]^{2+} \rightarrow 2[Cu^{II}_2O]^{2+} + O_2 \quad (7)$$

trations. Reactions like 6 and 7 are prevented by *physical immobilization* of dimeric copper sites in hemocyanins and tyrosinases.[4-6]

Our own work with *neutral* halo(amine)copper(I) complexes demonstrates the great tendency for complete dioxygen reduction under *ambient* conditions, eq 3–5.[6,13-15] Complete reduction causes the rate laws for reactions 3–5 to be a direct reflection of reductant molecularity.[13-15] For example, the irreversible third-order rate law 8 is observed for oxidation of excess neutral cop-

$$d[Cu^{II}_2O]/dt = k_D[Cu^I_2]^2[O_2] \quad (8)$$

per(I) dimers LCu(X,X)CuL (L is an *N,N,N′,N′*-tetraalkyldiamine; X is Cl or Br) by dioxygen, eq 5.[14,15] Rate law 8 demonstrates that two Cu^I_2 dimers, representing four available electrons, are required for irreversible dioxygen reduction.[13-15] This raises the question as to whether reactions 5 proceed in two separate steps, eq 9 and 10, and whether these steps are kinetically separable at low temperatures, where eq 2 has been demonstrated.[5,9-12]

$$Cu^I_2 + O_2 \rightarrow Cu^{II}_2O_2 \quad (9)$$

$$Cu^{II}_2O_2 + Cu^I_2 \rightarrow 2Cu^{II}_2O \quad (10)$$

This paper reports the stoichiometry and kinetics of oxidation of excess (TEED)Cu(Cl,Cl)Cu(TEED) (D) by dioxygen in methylene chloride in the temperature range −40.6 to −76.0 °C. It is the first successful attempt to obtain direct kinetic data for aprotic peroxocopper systems. The copper(I) reactant was selected for several reasons: (1) it is known to be a (μ,μ)-dichlorobridged dimer, with a copper–copper separation of 2.60 Å;[16] (2) we already have kinetic data for its oxidation at ambient temperatures with rate law 8;[15] (3) D and its oxidation product (TEED)Cu(Cl,-O,Cl)Cu(TEED) (C) are stable.[17] This is important because Thompson[12] observed that diamines with smaller *N*-alkyl substituents do not give reproducible primary oxidation products at low temperatures. We found that (a) the product of oxidation of $(en)_2Cu_2Cl_2$ (en = ethylenediamine) is very unstable at 25 °C,[7] (b) solutions of equimolar CuX and N,N′-dialkyldiamines in methylene chloride produce insoluble disproportionation products—even immediate reaction with dioxygen gives very unstable species—and (c) $(TMED)_2Cu_2Cl_2O$ is a rapidly polymerizing system at 5 °C in nitrobenzene.[15]

Our study indicates that blue tetrameric, mixed-valence peroxocopper species A forms in a third-order process and then equilibrates with another tetrameric form B at low temperatures (Scheme I). We also have deduced the kinetics of first-order decomposition of A to give 2 mol of the green ambient oxidation product C. It is concluded from low-temperature measurements that C is the initiator and catalyst for the oxidative coupling of 2,6-dimethylphenol to poly(2,6-dimethylphenylene oxide) by dioxygen.

Experimental Section

Materials. TEED (Aldrich) was freshly distilled under vacuum before use. Copper(I) chloride was prepared by the literature method.[18] 2,6-Dimethylphenol (POH; Aldrich) was used as received. Methylene chloride (Baker or American Burdick and Jackson) was purified as described previously.[13] High-purity dinitrogen was deoxygenated by passage through a freshly activated column of Alfa DEOX catalyst. Except as noted, solutions of D were prepared by adding solid CuCl to equimolar TEED in a known volume of methylene chloride under dinitrogen at room temperature. Density measurements enabled reactant concentrations to be calculated at each lower experimental temperature.

Scheme I

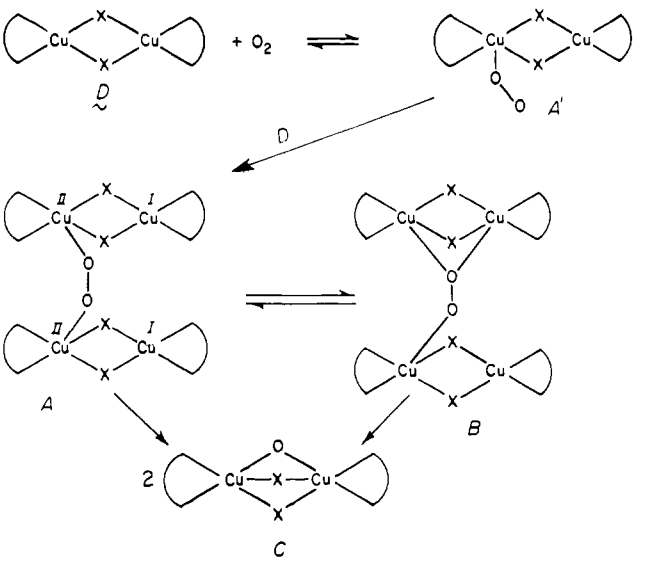

Stoichiometry Measurements. The stoichiometry of oxidation of D by dioxygen in methylene chloride was measured manometrically in a Warburg apparatus[15] as a function of [D] = (2.0–10.6) × 10^{-3} M at −76 and −45 °C.

Kinetic Measurements. Rates of formation of A and B were measured with our glass–quartz stopped-flow spectrophotometer, which is interfaced to a Digital Equipment PRO-350 computer with advanced acquisition, processing, and graphics capabilities.[15] The flow system was immersed in CO_2-solvent mixtures at −40.6, −50.1, −61.0, and −76.0 °C, with temperature controlled to ±0.2 °C. Spaces between the monochromator exit slit and entrance light pipe and between the exit light pipe and the photomultiplier housing were evacuated to prevent water condensation. Kinetic measurements were always made with sufficient excess [D] to ensure pseudo-first-order conditions.

Nature and Kinetics of Decomposition of A. Manometric measurements were used to show no net dioxygen evolution when a preformed solution of A, B[19,20] at −60 °C was allowed to warm to room temperature and then returned to −60 °C. Thus, A decomposes to C via eq 11 and not by disproportionation reaction 12.

$$A \rightarrow 2C \quad (11)$$

$$2A \rightarrow 2C + O_2 \quad (12)$$

Attempts were made to study the kinetics of reaction 11 in the temperature range −25 to −40 °C, where it can be determined whether the product of oxidation of D by O_2 at any particular temperature is A or C. Although direct kinetic measurements of reaction 11 were not possible because of the complexity of the system between −25 and −40 °C, we were able to account for a small temperature range over which the product changes from being A to being C (see below). Once this temperature range had been identified we were able to investigate whether A[20] or C was the better initiator for the oxidative coupling of 2,6-dimethylphenol by dioxygen.

Other Physical Measurements. Raman spectra were obtained with a Spex Model 1401 spectrometer (12-W Ar^+ laser (5145 Å); 500-mW incident power) coupled to a Spex Datamate processor. ESR measurements were made in methylene chloride solutions with a Varian E-9 instrument. The polymeric products of copper-catalyzed oxidative coupling of 2,6-dimethylphenol were characterized by size-exclusion chromatography with THF as the mobile phase on a Waters 244 ALC/GPC

(13) Davies, G.; El-Sayed, M. A. *Inorg. Chem.* **1983**, *22*, 1257.
(14) Churchill, M. R.; Davies, G.; El-Sayed, M. A.; Fournier, J. A.; Hutchinson, J. P.; Zubieta, J. A. *Inorg. Chem.* **1984**, *23*, 783.
(15) El-Sayed, M. A.; El-Toukhy, A.; Davies, G. *Inorg. Chem.* **1985**, *24*, 3387.
(16) Haitko, D. A.; Garbauskas, M. F. In *Biological and Inorganic Copper Chemistry*; Karlin, K. D., Zubieta, J., Eds.; Adenine: Guilderland, NY, 1986; Vol. 2, p 77 and references therein.
(17) Slow oxidation of the TEED ligands in C is observed at room temperature: see ref 12 and 14 and the text.
(18) Keller, R. N.; Wycoff, H. D. *Inorg. Synth.* **1946**, 2.
(19) An irreversible color change from blue to green is observed on heating A or B above ca. −40 °C (see text).
(20) Throughout this paper, references to A and B refer to equilibrium mixtures at various temperatures: for example, at −76 °C, [B]/[A] ≈ 13 from Table II.

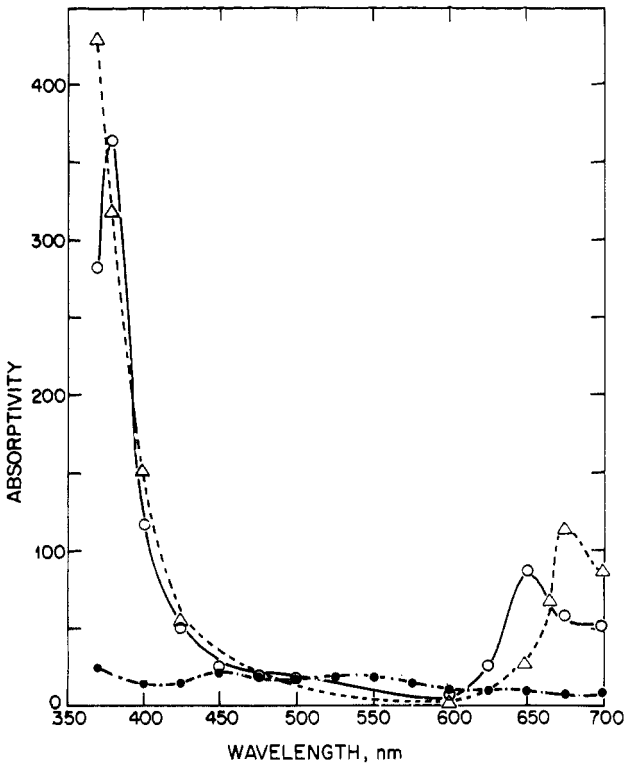

Figure 1. Electronic spectra of D (●), B^{20} (○), and C^{20} (△) at −76 °C in methylene chloride. Ordinate axis units are atomic copper absorptivities because B is a mixed-valence species (see text).

instrument with a Model 6000A solvent delivery system, a Model U6K injector, and a Model R400 refractive index (RI) detector coupled to a Spectra-Physics SP4000 data system. Additional chromatography was performed on a Waters 150 ALC/GPC instrument coupled to a Waters data module. The systems were calibrated with NBS standard samples of polystyrene.

Results and Discussion

Reaction Stoichiometry and Products. Colorless (TEED)Cu(Cl,Cl)(TEED) (D)[15,16] is air-sensitive as a solid and much more so in aprotic solvents.[15] Manometric dioxygen uptake measurements at 25 °C show that the stoichiometry of ambient reaction of D with dioxygen is given by eq 13, which indicates formation

$$2D + O_2 \rightarrow 2(TEED)_2Cu_2Cl_2O \qquad (13)$$

of oxocopper(II) by complete O_2 reduction.[15] Cryoscopic measurements show that the green oxocopper(II) product C is dimeric; its electronic spectrum (Figure 1 and ref 15) supports 5-coordinate copper(II) centers in a triply bridged structure, Scheme I.

Attempts to crystallize C are frustrated by its slow polymerization under dinitrogen[15] and by consumption of additional dioxygen, which results in oxidation of the ethyl substituents.[12,15] However, the latter process is too slow to interfere with kinetic measurements of copper(I) oxidation by O_2, which proceeds with rate law 8 at ambient temperatures.[15]

Low-Temperature Manometric Measurements. Manometric measurements showed that the stoichiometry of oxidation of D by dioxygen is $\Delta[D]/\Delta[O_2] = 2.0 \pm 0.2$ at $[D] = (2.0\text{–}10.6) \times 10^{-3}$ M at −76 and −45 °C. Precautions were taken to minimize cooling of the gas buret system by the reaction vessel contents. The dioxygen uptake behavior of blanks (equal volumes of methylene chloride solvent) was determined at the respective temperatures: the largest blank correction was −20% of the measured volume of dioxygen consumed by D at $[D] = 2.0 \times 10^{-3}$ M and −76 °C, where the rate of dioxygen uptake was lowest.

These results show that D reacts with dioxygen with the same stoichiometry either below −45 °C or at ambient temperatures. However, the respective blue and green solutions obtained (Figure 1) indicate the formation of different products, Scheme I.

We attempted to measure the molecular weight of blue product B by cryoscopy in methylene chloride (fp −99.5 °C) but found its solubility to be too low (ca. 10^{-3} m) to give significant freezing point depressions. We tried to obtain crystalline A and B by slow cycling of methylene chloride solutions between −45 and −80 °C, but only blue powders were obtained. Thompson[12] devised a complex procedure to obtain a solid that analyzed at room temperature as $[(TEED)Cu(O_2,H_2O)Cu(TEED)](ClO_4)_2$ but was unstable when redissolved. Our solids changed from blue to green C on warming to room temperature, but solid C soon became insoluble in methylene chloride at room temperature even under dinitrogen, presumably because of polymerization.[7,15] Our observations indicated that samples of B would have to be characterized at low temperature, and thus all spectral work was conducted with millimolar concentrations in methylene chloride.

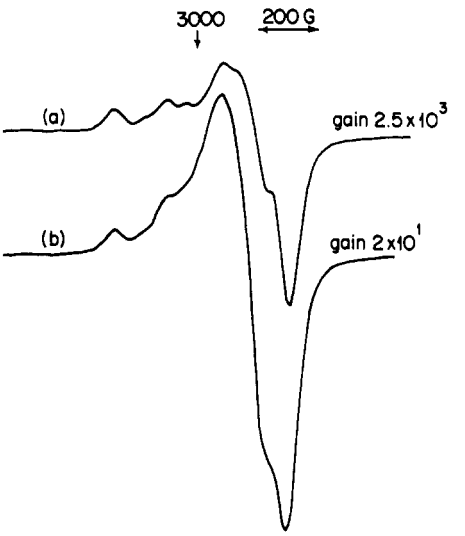

Figure 2. ESR spectra of (a) B and (b) C in methylene chloride glasses at 15 K; $2[B] = [C] \approx 2 \times 10^{-3}$ M.

Evidence for Mixed-Valence, Tetranuclear Peroxocopper Products at Low Temperatures. Our conclusion that A and B are mixed-valence tetranuclear peroxocopper species is based on (1) electronic, Raman, and ESR spectra, and (2) low-temperature kinetic data which suggest a tetranuclear product and require no molecularity variation for their interpretation. We therefore assign the manometric stoichiometry measurements at −76 and −45 °C to eq 14.

$$2D + O_2 \rightarrow [(TEED)_2Cu_2Cl_2]_2O_2 \qquad (14)$$

Electronic Spectra. The absorptivities of D, B, and C of Figure 1 are expressed in units of L (mol of Cu)$^{-1}$ cm^{-1} because B is a mixed-valence species (see below). Reactant D and oxo product C are known to be dimeric at ca. 5 °C;[15] their spectra at −76 °C agree with those at higher temperatures if the respective atomic absorptivities are multiplied by 2, which indicates that D and freshly prepared C are dimeric at 25 and −76 °C. The apparent weak maxima at 450 and 540 nm in Figure 1 are not observed in the spectrum of D at room temperature and are minor artifacts of the low-temperature measurements. They do not significantly alter our conclusions concerning the spectral features of C and B: green C has an absorption maximum at 675 (ϵ = 230 M^{-1} cm^{-1}),[15] and blue complex B has maxima at 380 and 650 nm (Figure 1). If B is accepted to be tetranuclear, then its molar absorptivities at these maxima are 1600 and 360 M^{-1} cm^{-1}, respectively.[21] Intense features near 380 nm have been observed in other peroxocopper(II) species[5,9,12] and are ascribed to $O_2^{2-} \rightarrow Cu^{II}$ charge transfer. The relatively low absorptivities for B at 380 and 650 nm are presumably due to its being a neutral, mixed-valence species (see below).[5,9-12]

ESR Spectra. Blue B and green C have different ESR spectra at 15 K (Figure 2). Seven, equally spaced hyperfine lines are discernible for B, but they are of unequal intensity and do not resemble the seven-line spectra for well-defined, electron-delo-

(21) Molar absorptivity ϵ_B estimated from eq 21 at −76 °C.

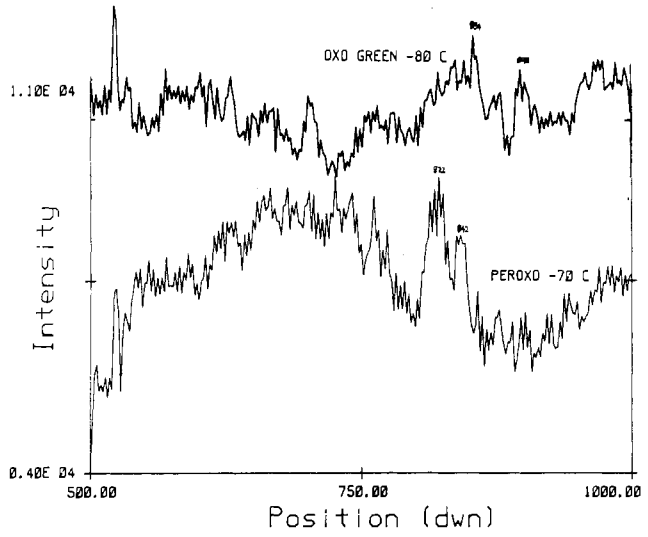

Figure 3. Low-temperature Raman spectra of B (bottom) and C (top). Note the prominent band at 822 cm^{-1} for B.

calized, mixed-valence copper complexes observed at higher temperatures.[22] The most prominent lines actually resemble those for C, which would be consistent with the proposed structure for B (Scheme I). This structure is also suggested by a broad, very weak low-field feature centered at $g = 4.33$ for B, which is more easily observed at $g = 3.77$ for C.

There is evidence for different peroxocopper species A and B at equilibrium between −76 and −50 °C (vide infra). Unfortunately, only isotropic spectra were observed for B and C at −80 °C ($\langle g \rangle = 2.11$ and 2.12, respectively), and no signals were measurable for either A, B, or C at −50 °C, presumably because of a sharp increase in spin–lattice relaxation rates with increasing temperature. For this reason, no independent evidence for equilibration between A and B or for mixed-valence peroxocopper species could be obtained from higher temperature ESR measurements.

Raman Spectra. The lower Raman spectrum in Figure 3 of the blue product B (Scheme I) formed at −76 °C in methylene chloride was measured at −70 °C with a Spex Raman spectrometer.[23] The reproducible, prominent band centered at 822 cm^{-1} (satellite at 842 cm^{-1}) is in the region assigned to ν_{O-O} in peroxocopper(II) complexes.[4,5,9-12] These bands were reproducible and unchanged at −100 °C but were irreproducible at −60 °C; they could not be observed at all at −50 °C, presumably because of laser-induced decomposition (A,B is thermally stable to ca. −40 °C (see below)). The different upper spectrum of the oxocopper(II) product C was obtained by warming the −76 °C product sample to room temperature and then rerecording the spectrum at −80 °C. Although experiments with $^{18}O_2$ as the oxidant would be confirmatory, it is very likely that the 822- and 842-cm^{-1} features are due to ν_{O-O} in A,B.[4,5,9-12]

Low-Temperature Kinetics. We used our stopped-flow equipment[15] to obtain kinetic data for reaction 14. Fixed temperatures of −76.0, −61.0, −50.1, and −40.6 °C were set by immersing the glass–quartz flow system in various dry ice/solvent mixtures.

Two well-resolved, reproducible reactions are observed at 380 nm on mixing excess D (2.0–10.6) × 10^{-3} M with dioxygen in methylene chloride at temperatures up to −50.1 °C (Figure 4).

The first reaction (product A) was irreversible (at fixed $[O_2]$ the absorbance change ΔA was independent of temperature up to −40.6 °C). Plots of ln $(A_\infty - A_t)$ vs. time, where A_t is the absorbance at time t, were linear to at least 4 half-lives at fixed excess [D] and temperature, showing that this reaction is first order in $[O_2]$. Plots of the pseudo-first-order rate constant,

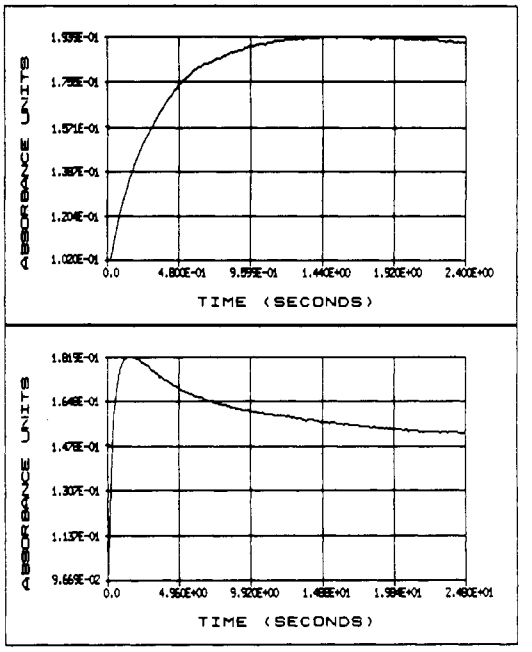

Figure 4. Absorbance–time records (380 nm) for reaction of D (1.06 × 10^{-2} M) with O_2 (6.7 × 10^{-4} M) in methylene chloride at −76 °C.

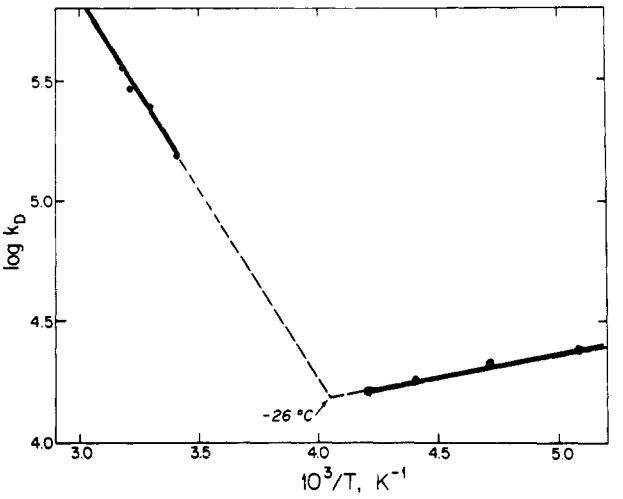

Figure 5. Temperature dependence of ambient (k_D, eq 8) and low-temperature (k_{DL}, eq 15) data for reaction of D with O_2 in methylene chloride. See text for discussion of extrapolated region.

Table I. Kinetic Data for the Low-Temperature Oxidation of Excess D to A by Dioxygen in Methylene Chloride (Eq 15)[a]

temp[b]	$10^{-4}k_{DL}$[c]	temp[b]	$10^{-4}k_{DL}$[c]
−76.0	2.46 ± 0.11	−50.1	1.88 ± 0.08
−61.0	2.12 ± 0.09	−40.6	1.80 ± 0.06

$\Delta H_{DL}^{\ddagger} = -1.0 \pm 0.3$ kcal mol^{-1}; $\Delta S_{DL}^{\ddagger} = -43 \pm 4$ cal deg^{-1} mol^{-1}

[a] Estimated standard deviations in parentheses; See ref 15 for corresponding data at higher temperature. [b] Given in °C. [c] Units are M^{-2} s^{-1} in rate law 15.

$k_{obsd}(15)$, vs. $[D]^2$ were linear and passed through the origin, establishing irreversible rate law 15. Kinetic data are given in Table I.

$$d[A]/dt = k_{DL}[D]^2[O_2] \quad (15)$$

The order of rate law 15 is significant for two reasons. First, it indicates that reactions 9 and 10 (Introduction) are not kinetically separable even at −76 °C. Second, it is of the same form as rate law 8 at ambient temperatures[15] (see below).

We find $\Delta H_{DL}^{\ddagger} = -1.0 \pm 0.3$ kcal mol^{-1} and $\Delta S_{DL}^{\ddagger} = -43 \pm 4$ cal deg^{-1} mol^{-1} at 25 °C for formation of product A (Figure 5). The simplest explanation for the negative activation enthalpy

(22) Gagnē, R. R.; Henling, L. M.; Kistenmacher, T. J. *Inorg. Chem.* **1980**, *19*, 1226 and references therein. Long, R. C.; Hendrickson, D. N. *J. Am. Chem. Soc.* **1983**, *105*, 1513.

(23) [B]/[A] is estimated to be ca. 11 at −70 °C (Table II).

Table II. Data for Equilibration of A and B in Methylene Chloride[a]

temp[b]	k_f[c]	k_r[c]	K_{19}
−76.0	0.28 (2)	0.021 (3)	13 (4)
−61.0	0.28 (2)	0.038 (4)	7 (3)
−50.1	0.24 (2)	0.060 (4)	4 (1)

$\Delta H_f^* = 0$ (0.3);[d] $\Delta S_f^* = -62$ (5);[e] $\Delta H_r^* = 3.3$ (6);[d] $\Delta S_r^* = -44$ (5);[e] $\Delta H_{19} = -3.3$ (6);[d] $\Delta S_{19} = -15$ (8)[e]

[a] Estimated standard deviations of last figure in parentheses. [b] Given in °C. [c] Units are s^{-1}. [d] Units are kcal mol^{-1}. [e] Units are cal deg^{-1} mol^{-1}.

ΔH_{DL}^* is a minor exothermic equilibrium 16 preceding rate-determining step 17 (see below). With this assumption $\Delta H_{DL}^* =$

$$D + O_2 \rightleftharpoons DO_2 \quad \Delta H_{16} < 0 \tag{16}$$

$$DO_2 + D \xrightarrow{k_{17}} A \quad \text{slow} \tag{17}$$

$\Delta H_{16} + \Delta H_{17}^* = -1.0$ kcal mol^{-1}. The very negative $\Delta S_{DL}^* = \Delta S_{16} + \Delta S_{17}^*$ is consistent with an associative mechanism.[13-15] However, rate law 15 indicates that the equilibrium constant for reaction 16 is too small to measure kinetically at −76 °C: $K_{16}[D] \lesssim 0.1$ at highest [D] gives $K_{16} \lesssim 10$ M^{-1}.[15] This is an indication that structure *A'* (Scheme I) or variants are thermodynamically unstable even at −76 °C (see below).

The second reaction observed (Figure 4) has rate law 18, where A is the product of reaction 17. Independence of rate law 18

$$\text{rate} = k_R[A] \tag{18}$$

on [D] confirms that reaction 17 is complete and irreversible and suggests that the absorbance decrease is due to relaxation between two product forms A and B, eq 19 (Scheme I). A progressive decrease in the total absorbance change ΔA associated with at-

$$A \underset{k_r}{\overset{k_f}{\rightleftharpoons}} B \quad \Delta H_{19} < 0 \tag{19}$$

tainment of equilibrium 19 occurred with increasing reaction temperature, −76.0 to −50.1 °C, indicating that system 19 is exothermic and reversible.

Equilibrium constants $K_{19} = k_f/k_r$ were independently obtained from the absorbances at 380 nm at three temperatures as follows.

Relaxation, eq 19, was not observable in our equipment (0.33-cm fixed path length) at temperatures above −50 °C. At −50 °C the measured absorbance Ab_1 at 380 nm from reaction 17 of excess D with a known concentration of dioxygen to give A leads to ϵ_A from eq 20, where $l = 0.33$ cm. If A relaxes

$$\epsilon_A = \frac{Ab_1}{[O_2]l} \tag{20}$$

completely to B at −76 °C,[24] then ϵ_B can be calculated from eq 21, where Ab_2 is the measured absorbance when system 19 is

$$\epsilon_B = \frac{Ab_2}{[O_2]l} \tag{21}$$

equilibrated. At higher fixed temperatures the extent of equilibration to B is less and the measured absorbance after relaxation, Ab_{2e}, is now given by eq 22, which can be rearranged to eq 23.

$$Ab_{2e} = \frac{[O_2](\epsilon_A + \epsilon_B K_{19})l}{1 + K_{19}} \tag{22}$$

$$K_{19} = \frac{\epsilon_A[O_2]l - Ab_{2e}}{Ab_{2e} - \epsilon_B[O_2]l} \tag{23}$$

Values of K_{19} calculated from eq 23 are given in Table II, together with k_f and k_r, eq 19, calculated from measured $k_R = k_f + k_r$ and $K_{19} = k_f/k_r$. The data in Table II confirm that equilibrium 19 is exothermic and give $\Delta H_{19} = -3.3 \pm 0.6$ kcal mol^{-1}, with $\Delta S_{19} = -15 \pm 8$ cal deg^{-1} mol^{-1} at 25 °C.

The measured stoichiometry, eq 14, and rate laws 15 and 18 strongly suggest that A and B both are constructed from *two* molecules of dimer D and one O_2 molecule, presumably due to the reluctance of O_2 to bridge the two copper centers in a single molecule of dimer D (Cu–Cu = 2.60 Å).[5,6,16] This is very probably why the equilibrium constant for reaction 16 is too small to measure even at −76 °C, while A forms irreversibly.

The data in Table II indicate that the activated complex for reaction 19, $(A,B)^*$, is more ordered than A and B, with the entropies decreasing $A > B \gg (A,B)^*$. We suggest the symmetrical structure

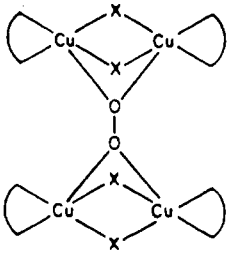

shown here for $(A,B)^*$. Its conversion to B is exothermic (−3.3 ± 0.6 kcal mol^{-1}), despite a requirement for Cu–O bond-breaking to give the proposed structure for B (Scheme I). Perhaps the strength of Cu–Cl bonds increases in this process.

As indicated in Scheme I, we believe that A and B are peroxocopper complexes. The decrease in absorbance at 380 nm (Figure 4) in reaction 19 presumably is due to greater charge delocalization in B.

The existence of A and B indicates a significant activation barrier for the transfer of a third electron from copper(I) to coordinated peroxide. This transfer would result in irreversible breaking of the O–O bond of A to give 2 mol of C, eq 11. We shall see why this third electron is not transferred at significant rates below −45 °C.

Kinetics of Conversion of A to C. The combined low and higher temperature data for rate laws 15 and 8,[15] respectively, Figure 5, have been extrapolated and intersect at −26 ± 6 °C. This is the theoretical temperature at which A and C are supposed to form at the same rate, but it is an illusion because C can only form from A or B via reaction 11. Kinetic studies of this process near −25 °C are complicated by the presence of approximately equal proportions of A and B predicted from K_{19} data in Table II. Because the rate of equilibration of A and B could be a complicating factor at −25 °C, we first made careful spectral observations in the temperature range −40 to −25 °C. The complexity of the system made it necessary to develop a kinetic model to explain our observations.

Spectral Observations. Dioxygen was passed for 30 min through a 2×10^{-3} M solution of D in a large Dewar vessel at −76 °C, resulting in oxidation of D to give a blue solution, predominantly of B (Table II).[20,24] Dinitrogen was then passed through the solution for 30 min as it was slowly allowed to warm to −50 °C. It was held there to confirm that A and B are not converted to D and O_2 or to C (reaction 11) at appreciable rates at −50 °C. Warming at 0.25 °C/min was then commenced as in a careful melting point determination. At −36 °C we observed a sharp color change from pale blue to darker green over a period of 1–2 s. This color change was not reversed by rapid cooling, and the spectra at −76 °C indicated that ca. 70% of irreversible reaction 11 had occurred at −36 °C in a very short time period.

The experiment was repeated, but now the system was rapidly (10 °C/min) heated to −30 °C and then immediately and rapidly cooled to −76 °C. Comparison of the resulting solution with a sample at −76 °C that had not been heated indicated that the heating experiment had resulted in complete reaction 11 in a very short time at −30 °C.

Repetition of the above two experiments with $[D] = 3 \times 10^{-3}$ M identified the temperature range −39 to −32 °C where a rapid, irreversible and highly temperature-dependent conversion of A/B to C occurs via reaction 11.

Attempted Measurement of the Kinetics of Reaction 11. The observations of the previous section and the spectra in Figure 1 suggest that reaction 11 might be kinetically observable at 650

(24) The data in Table II indicate that this assumption is good to ±10%.

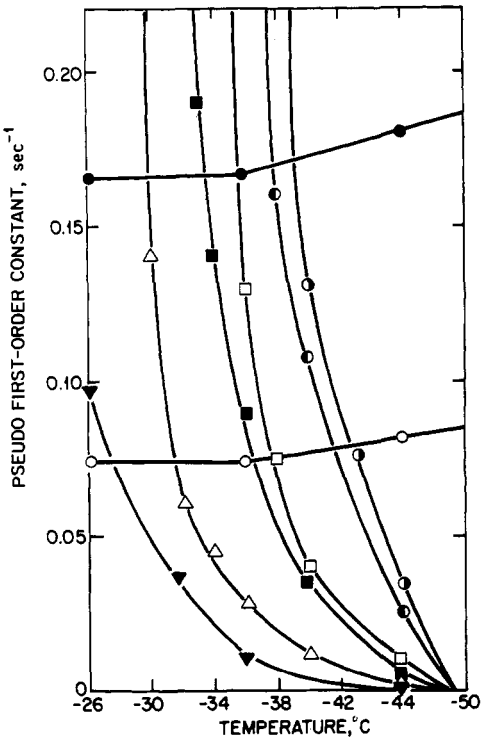

Figure 6. Comparison of the temperature dependences of $k_{obsd}(15)$ (s^{-1}) at [D] = 2×10^{-3} M (○) and 3×10^{-3} M (●) with k_{11} (s^{-1}) calculated with the following values of $\Delta H_{11}^{\ddagger}$ (kcal mol^{-1}) and $\Delta S_{11}^{\ddagger}$ (cal deg^{-1} mol^{-1}): (▽) 25.5, 40; (△) 25.0, 40; (■) 24.5, 40; (□) 25.5, 45; (◐) 24, 40; (◑) 25, 45.

or 675 nm in the temperature range −39 to −32 °C. However, only one exponential process was observed when D (2×10^{-3} M) was reacted with O_2 (2.0×10^{-4} M) at either −40 or −32 °C.

The difficulties in kinetic monitoring of reaction 11 in the critical temperature range are probably due to practical and chemical factors. We found in practice that long-term temperature control with a 4-L flow system thermostat and mixed solvent/dry ice or N_2 slush baths was much less precise (±1.0 °C) than at lower temperatures. The second practical requirement is high spectral resolution. Thus, according to the data in Figure 1, reaction 11 should result in a 4-fold decrease in absorbance at 650 nm but a 2.4-fold increase at 675 nm; at 660 nm essentially no absorbance change due to reaction 11 would be predicted. We observed simple exponentials at 650 and 675 nm in the "critical" region in which reaction 11 occurs.

The first chemical factor is possible spectral interference from equilibration of A and B in the critical temperature range (K_{19} is calculated (from Table II) to be 2 ± 1 and 1 ± 1 at −40 and −30 °C, respectively): as mentioned earlier, although equilibration 19 is not directly observable at temperatures above −50 °C, it could cause reaction traces to be pseudoexponential. The second chemical factor is a temperature-insensitive pseudo-first-order rate constant $k_{obsd}(15)$ but a highly temperature-sensitive first-order rate constant $k_{obsd}(11)$ (see discussion below).

Deduction of Kinetic Parameters for Reaction 11. We adopted the following approach to account for the obvious strong kinetic temperature dependence of reaction 11. The conversion of A to C was assumed to be a first-order process with k_{11} given by eq 24, where the symbols have their usual significance.[25] Values

$$k_{11} = (kT/h) \exp(-\Delta H_{11}^{\ddagger}/RT) \exp(\Delta S_{11}^{\ddagger}/R) \quad (24)$$

of k_{11} were generated from eq 24 with $\Delta H^{\ddagger}$ = 0–45.0 kcal mol^{-1} (in steps of 0.3 kcal mol^{-1}) and $\Delta S_{11}^{\ddagger}$ = −70 to +130 cal deg^{-1} mol^{-1} (in steps of 2 cal deg^{-1} mol^{-1}) at −26 and −46 °C. At each $\Delta H_{11}^{\ddagger}$, the upper limit of $\Delta S_{11}^{\ddagger}$ that permitted k_{11} to be as high as 0.03 s^{-1} at −46 °C (see Figure 6) was recorded as $\Delta S_{11u}^{\ddagger}$: for example, at $\Delta H_{11}^{\ddagger}$ = 10.2 kcal mol^{-1}, we have $\Delta S_{11u}^{\ddagger}$ = −22 cal deg^{-1} mol^{-1} with this criterion. Inspection of all the calculated k_{11} values gave the lowest value, $\Delta S_{11l}^{\ddagger}$, required to predict $k_{11} \gtrsim 2$ s^{-1} at −26 °C (see Figure 6) at any particular $\Delta H_{11}^{\ddagger}$. The function DIFF = $\Delta S_{11l}^{\ddagger} - \Delta S_{11u}^{\ddagger}$ was then plotted vs. $\Delta H_{11}^{\ddagger}$.[26] If k_{11} is a first-order rate constant then $\Delta S_{11l}^{\ddagger}$ and $\Delta S_{11u}^{\ddagger}$ will be one and the same.

The results in the supplementary figure[26] show that DIFF = 0 when $\Delta H_{11}^{\ddagger}$ = 25.0 ± 0.5 kcal mol^{-1}, which also requires $\Delta S_{11}^{\ddagger}$ = 40 ± 3 cal deg^{-1} mol^{-1} to explain the observed behavior of the D/O_2 system at −26 °C (production of C) and −46 °C (production of A,B).

Kinetic Consequences. The results in Figure 6 with $\Delta H_{11}^{\ddagger}$ = 25 kcal mol^{-1} and $\Delta S_{11}^{\ddagger}$ = 40 cal deg^{-1} mol^{-1} show that $k_{obsd}(11)$ is 0.037, 1.3, and 1.8 times $k_{obsd}(15)$ at −46, −32, and −30 °C, respectively, at [D] = 2×10^{-3} M. The predicted "critical" temperatures are −32 and −30 °C at [D] = 2 and 3×10^{-3} M, respectively. The predictions also agree with our observations that A,B[20] and C are the exclusive products of oxidation of D by O_2 at −46 °C and −26 °C, respectively.

From Table II we can calculate that k_R for equilibrium 19 is 0.30, 0.36, and 0.39 s^{-1}, while k_r is 0.06, 0.12, and 0.15 s^{-1}, at −46, −36, and −26 °C, respectively. The values for k_r confirm that B → A equilibrium 19 contributes to the phenomena observed in the critical temperature range. However, because of the relatively slight temperature dependence of k_r, we still have to invoke a strong temperature dependence of k_{11} to explain the appearance of C at −26 °C and A,B at −46 °C.

We now understand why the lines in Figure 5 intersect near −26 °C: at this temperature the rate of reaction 11 is much higher than that of 14, and the observed product is the green oxocopper(II) complex C. We can also conclude that O–O bond-breaking reaction 11 is not the rate-determining step in the reaction of D with O_2 under ambient conditions as follows.

At 21 °C, $k_{calcd}(11) = 1.8 \times 10^3$ s^{-1} [27] while the observed pseudo-first-order rate constant for rate law 8 at [D] = 2×10^{-3} M is 8×10^{-3} s^{-1} from the data in ref 15. Thus, the sterically controlled activated complex assembly is the rate-determining step in reaction 5, as concluded earlier from comparison of solvent and activation parameter variations in rate law 8.[15]

We have no strong feelings about the magnitude assigned to $\Delta H_{11}^{\ddagger}$, 25 kcal mol^{-1}; it is somewhat lower than those found for homolytic O–O bond breaking in peroxides such as diacetyl peroxide ($\Delta H^{\ddagger}$ = 28.9 kcal mol^{-1}) and dialkyl peroxides ($\Delta H^{\ddagger}$ averages ca. 36 kcal mol^{-1}).[28] However, direct comparison is not straightforward because A and B are neutral, mixed-valence metal species and reaction 11 is "intramolecularly electron-assisted."

On the other hand, $\Delta S_{11}^{\ddagger}$ = 40 cal deg^{-1} mol^{-1} is quite reasonable for an activation process that involves O–O bond breaking in A,B to give 2 mol of C in a weakly coordinating, aprotic solvent.[13,29]

Observations in the Presence of 2,6-Dimethylphenol. Oxocopper(II) complex C and related halo(amine)copper(II) complexes containing oxo or carbonato groups are active initiators for the oxidative coupling of phenols by dioxygen, eq 25.[2,15,16]

(25) It is recognized at this point that k_{11} is a composite, first-order rate constant for the conversion of A or B to C. The system is too kinetically complicated in the −30 to −40 °C temperature range to allow distinction of individual rates.

(26) Supplementary data. At fixed $\Delta H_{11}^{\ddagger}$, the effect of imposing a smaller upper limit on k_{11} at −46 °C is to decrease $\Delta S_{11u}^{\ddagger}$, which increases DIFF. However, this has no net effect on the intercept, $\Delta H_{11}^{\ddagger}$ = 25.0 ± 0.5 kcal mol^{-1}, in the supplementary figure.

(27) k_{11} is estimated at 21 °C from $\Delta H_{11}^{\ddagger}$ = 25 kcal mol^{-1} and 40 cal deg^{-1} mol^{-1} (see Figure 6 and text).

(28) Raley, J. H.; Rust, F. F.; Vaughan, W. E., *J. Am. Chem. Soc.* **1948**, *70*, 88, 1336, 2767. Szware, M. In *Peroxide Reaction Mechanisms*; Edwards, J. O., Ed.; Wiley-Interscience; New York; 1962, p 164.

(29) It seems intuitively reasonable that reaction 11 would proceed preferentially by inner-sphere electron transfer from formal copper(I) to peroxide in B; this suggestion is tentative in the complicated D/O_2 system of the present study but might be kinetically verifiable in D systems containing different L and X.

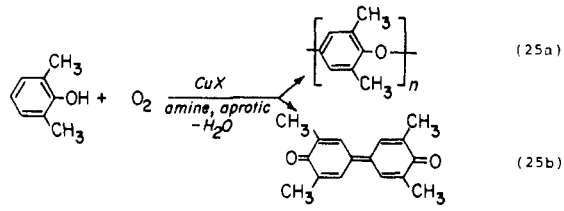

(25a)

(25b)

It is well-known that highly active initiators result from aprotic oxidation of dimers such as D with dioxygen. Catalysis probably results from shuttling between copper(I) and copper(II), with copper(II) acting as the oxidant of phenolate. The latter is likely produced by deprotonation of phenol by basic sites in species like A, B, or C.[2,15,16]

The experiments to be described were directed at answering the following questions. First, do reactions 25 occur at temperatures below −40 °C, where oxidation of D gives peroxocomplexes A and B? If so, what is the rate and final product distribution (polymer/quinone)? Second, since oxidation of D by O_2 gives C at temperatures above −26 °C (Figure 5), how do the rates of phenol oxidation and the product distributions vary with temperature in the range −76 to 0 °C?

All of the experiments were carried out with [D] = 2×10^{-3} M and 2,6-dimethylphenol (POH), [POH] = 4×10^{-2} M, each in methylene chloride (30 mL). We observed a pale violet color when these solutions were mixed at −76 °C under dinitrogen but not at −25 °C (see below).

Addition of the POH solution to B at −76 °C under dinitrogen gave an immediate color change to deep violet (λ_{max} = 530, 600, 700 sh nm, Figure 7). Heating the solution to −45 °C under dinitrogen caused the violet color to fade. Introduction of a continuous flow of dioxygen at −41 °C rapidly regenerated the violet spectrum in Figure 7. The temperature of the mixture was allowed to rise slowly above −40 °C under dioxygen. At ca. −35 °C it sharply changed (inset) to pale brown (λ_{max} = 760 nm, Figure 7) and remained brown to −26 °C. However, rapid recooling to −40 °C regenerated the violet spectrum. Rapid cycling between −40 and −26 °C could be repeated with reproducible, sharp color changes until the solution was green, at which time the solution also was green (C) at −76 °C. Finally, the solution was evaporated to half-volume under vacuum at room temperature and treated with 0.5 M HCl in methanol (50 mL). The precipitated polymer (reaction 25a) was washed twice with 5 mL of the HCl solution, dried overnight at 110 °C, and weighed. The isolated yield was 0.132 g (95%) and M_w from size exclusion chromatography was 2.6×10^4 ($M_n = 1.6 \times 10^4$).

We next investigated the reaction of A,B with POH under a continuous flow of dioxygen at −45 °C. A color change from violet (Figure 7) to green after 3 h signaled consumption of all POH. The solution was treated as above to obtain the diphenoquinone product of eq 25b, identified by comparison with an authentic sample; isolated yield 0.091 g (66%).

Catalyzed phenol oxidation was found to be very slow at lower temperatures; negligible yields of polymer and diphenoquinone were obtained in 2 days at −50 and −76 °C.

These experiments suggest that the peroxocopper species A and B initiate and probably catalyze reaction 25b, but at very low rates below −50 °C.

The experiments were repeated exactly as above but at −25 and 0 °C. Initiator C was freshly prepared by reaction of D with O_2 at these respective temperatures. At −25 °C the reaction was over in 13 min and gave a 95% isolated polymer yield ($M_w = 2.1 \times 10^4$). The corresponding results at 0 °C were 38 min, 96%, and 3.3×10^4, respectively. These experiments show that oxocopper(II) complex C initiates and very probably catalyzes reaction 25a and that M_w is essentially temperature-independent.

We offer Scheme II to explain our observations.

The left cycle operates at temperatures above ca. −30 °C. Although no color change is observed on mixing D with POH, we allow for reversible coordination of POH by D. Oxidation of D and D(POH)$_m$ by O_2 gives pale brown C(PO)$_n$ (lower spectrum in Figure 7), which reacts with POH in eq 25a to give the colorless

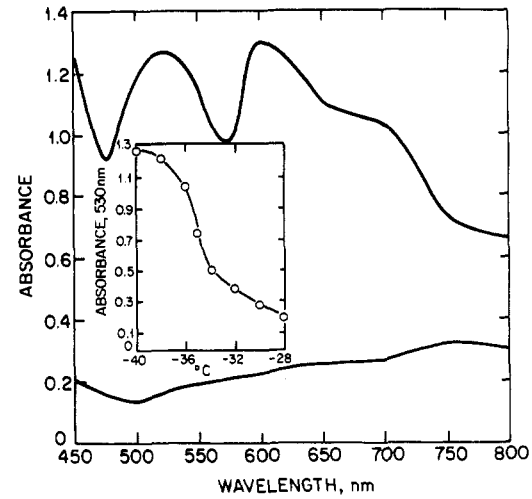

Figure 7. Electronic spectra: upper spectrum, B(OP)$_n$ in methylene chloride at −60 °C; lower spectrum, same sample at −26 °C. The inset shows the temperature dependence of absorbance at 530 nm (upper spectrum) between −40 and −28 °C. The heating rate is 5 °C/min. The product spectrum is the lower spectrum.

Scheme II

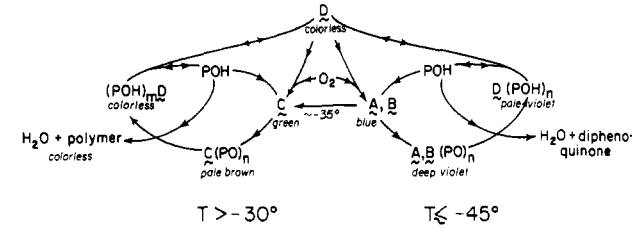

product poly(2,6-dimethylphenylene oxide) and colorless D-(POH)$_m$. Green oxocopper(II) (or a green hydrated form[30]) is the resting state of copper(II) under dioxygen in this cycle.

The right cycle operates at −45 °C or lower temperatures and is based on oxidation of D and pale violet D(POH)$_n$ by O_2 to deep violet A,B(PO)$_n$. Very slow reaction of the latter with POH gives predominantly the diphenoquinone product, eq 25b, at −45 °C. Blue system 19 (or a hydrated form[30]) is the resting state of this cycle under dioxygen.

These cycles are linked by the rapid conversion of A,B to C at ca. −35 °C (inset of Figure 7), precisely as demonstrated in the absence of POH. The colors and products observed in an operating catalytic cycle thus essentially depend on whether D is oxidized to A, B or C, which, in turn, depends on the experimental temperature.

Conclusions. The products of oxidation of D with O_2 in methylene chloride depend on the experimental temperature. Blue peroxocopper products A and B are formed irreversibly from D and O_2 at low temperatures. These species decompose irreversibly to the green oxocomplex C over a narrow temperature range (ca. −40 to −30 °C) via the highly temperature-dependent reaction 11. It will be interesting to see if reaction 11 can be monitored directly in dimers D containing different L and X.[29]

It appears that involvement of A, B, and C in the catalyzed reaction of 2,6-dimethylphenol with dioxygen leads predominantly to diphenoquinone and polymer products, respectively. It is possible that higher proportions of diphenoquinone products at temperatures above 0 °C[15] arise from adventitious involvement of A,B(PO)$_n$, rather than exclusive C(PO)$_n$, at very high phenol concentrations. Our observations suggest that different oxidation states of dioxygen lead to different phenolic oxidation products,

(30) This caveat allows for the likely interaction of B and C with water, the coproduct of eq 25, which will alter the nature of progressive catalyzed phenol oxidation. Symbols like D(POH)$_n$ in Scheme II represent only their constituent parts. We have no independent information on their molecularity, which could vary with experimental conditions.

but they provide no information on the identity or fate of species between $A,B(PO)_n$ or $C(OP)_n$ and final products.

Acknowledgment. This work was supported financially by Grant RR07143 from the Department of Health and Human Services and by Grant INT-8512210 from the National Science Foundation, which are gratefully acknowledged. We thank Professors Ahmed El-Toukhy, John Groves, and Kenneth Karlin for valuable discussions, Professor Conrad Jankowski for software development, Marie Kayser-Potts and Dr. Michael Sennett for M_w and Raman measurements, Professor William Orme-Johnson and co-workers for help with ESR measurements, Digital Equipment Corp. for donation of the PRO-350 computer and peripherals, and Dr. Mark Schure for system programming. Finally, M.A.E.-S. thanks Alexandria University for study leave.

Registry No. D, 97731-71-0; 2,6-dimethylphenol, 576-26-1.

Supplementary Material Available: Plot of 10^3DIFF (kcal deg^{-1} mol^{-1}) vs. $\Delta H_{11}^{\bullet}$ (kcal mol^{-1}) (1 page). Ordering information is given on any current masthead page.

Contribution from the University Chemical Laboratory, Cambridge CB2 1EW, U.K.

Ligand Fields from Misdirected Valency. 4. Magnetic Susceptibilities and Electron Spin Resonance and Optical Spectra of Tetrakis(diphenylmethylarsine oxide)(nitrato)cobalt(II) and -nickel(II) Nitrates

Neil D. Fenton and Malcolm Gerloch*

Received March 5, 1987

Ligand-field analyses of $[M(OAsPh_2Me)_4NO_3]^+NO_3^-$ (M = Co(II), Ni(II)) have accurately and simultaneously reproduced the principal crystal susceptibilities and their temperature variations in the range 80–300 K, the d–d optical transition energies, and, for the cobalt complex, the principal molecular g values and their orientations. A cellular ligand-field approach has been based upon a recent crystallographic reanalysis. Substantial values for local $e_{\pi\sigma}$ parameters for both ligand types evidence the misdirected nature of the local metal–oxygen interactions arising from bent bonding and/or contributions from oxygen nonbonding lone pairs. Detailed differences between values of $e_{\pi\parallel}$ (referring to the misdirected valence) are argued to reflect slightly more polarization of the metal–oxygen bonds toward the nickel atom than toward the cobalt. The same greater effective nuclear charge in the d^8 complex is accompanied by a relative increase in the axial metal–oxygen bonding and ligand field in that complex.

Introduction

In 1965 the preparation of the complexes $M(Ph_2MeAsO)_4X_2$ (M = Co(II), Ni(II); X = NO_3^-, ClO_4^-) was reported,[1] together with a preliminary X-ray structural analysis[2] that characterized their pentacoordination geometry as being of the square-based pyramidal type. One nitrate or perchlorate group bonds to the metal atom in the apical site while the other forms an anion of crystallization. Since then extensive studies of all important ligand-field properties of these molecules have been investigated. The paramagnetic susceptibilities and anisotropies of the tetragonal crystals have been measured[3,4] in the temperature range 300–80 K for the nitrate complexes of both metals together with single-crystal, polarized optical spectra[3,4] at 20, 80, and 300 K. More recently, Bencini et al.[5] have presented a careful study of the single-crystal ESR **g** tensors of $[Co(Ph_2MeAsO)_4NO_3]^+NO_3^-$. The early X-ray study placed the metal atoms in these complexes on crystal tetrads, so requiring disorder of the apical perchlorate or nitrate donors. The ESR study monitored the ensuing lower molecular symmetry uniquely within the ligand-field measurements, revealing a very large in-plane anisotropy for the **g** tensor.

Hitherto, two ligand-field analyses have been published. The earlier one[3,4] reproduced the principal crystal susceptibilities and d–d transitions in the optical spectra within the global and approximate parameterization scheme in fourfold symmetry in terms of variables such as *Dq*, *Ds*, and *Dt*. The potentially much more revealing parameterization of the Angular Overlap Model (AOM) was employed by Bencini et al.[5] in the more recent study. A good account of the principal g values and their orientations was provided for the cobalt system, but only fair reproduction of the optical spectrum was achieved. The correct sign of the crystal paramagnetic anisotropy was predicted, but quantitative agreement with experiment was lacking. The "best-fit" AOM parameter set was reported[5] as follows: $e_\sigma(NO_3)$ = 6015 cm^{-1}, $e_{\pi\perp}(NO_3)$ = 1580 cm^{-1}, $e_{\pi\parallel}(NO_3)$ = 3950 cm^{-1}, e_σ(AsO) = 6685 cm^{-1}, e_π(AsO) = 2765 cm^{-1}, B = 760 cm^{-1}, k = 0.9, ζ = 533 cm^{-1}. Shortcomings of this analysis are apparent in the use of an isotropic treatment for e_π(AsO); the very large value of the ligand-field trace Σ (defined[6,7] as the sum of all diagonal e values in a given complex) of 60 405 cm^{-1} as compared with values around 22 000 cm^{-1} for many other cobalt(II), nickel(II), and copper(II) systems;[8] and the neglect of the misdirected nature of all the metal–oxygen interactions in these species. Earlier papers[9-11] in this series have established the need to recognize both bent bonding and the role of nonbonding donor-atom long pairs in ligand-field studies. Their neglect can affect both the efficacy and significance of such analyses markedly.

The present analysis seeks to provide good agreement with all experimental ligand-field properties and achieves this in a manner that is consistent with a wide and growing body of similar ligand-field analyses within what we now call the Cellular Ligand-Field (CLF) model.

(1) Lewis, J.; Nyholm, R. S.; Rodley, G. A. *Nature (London)* **1965**, *207*, 72.
(2) Pauling, P.; Robertson, G. B.; Rodley, G. A. *Nature (London)* **1965**, *207*, 73.
(3) Gerloch, M.; Kohl, J.; Lewis, J.; Urland, W. *J. Chem. Soc. A* **1970**, 3269.
(4) Gerloch, M.; Kohl, J.; Lewis, J.; Urland, W. *J. Chem. Soc. A* **1970**, 3283.
(5) Bencini, A.; Benelli, C.; Gatteschi, D.; Zanchini, C. *Inorg. Chem.* **1979**, *18*, 2526.
(6) Deeth, R. J.; Gerloch, M. *Inorg. Chem.* **1985**, *24*, 1754.
(7) Woolley, R. G. *Chem. Phys. Lett.* **1985**, *118*, 207.
(8) Deeth, R. J.; Gerloch, M. *J. Chem. Soc., Dalton Trans.* **1986**, 1531.
(9) Deeth, R. J.; Duer, M. J.; Gerloch, M. *Inorg. Chem.* **1987**, *26*, 2573.
(10) Deeth, R. J.; Duer, M. J.; Gerloch, M. *Inorg. Chem.* **1987**, *26*, 2578.
(11) Deeth, R. J.; Gerloch, M. *Inorg. Chem.* **1987**, *26*, 2582.

0020-1669/87/1326-3273$01.50/0